

Chapter 2

Channel Backscattering Theory and Modeling

2.1 Introduction

As the mobility degradation and process complexities become the bottleneck for device scaling, to target the drive current and device performance according to the international technology roadmap for semiconductors (ITRS) [2.1], there are a lot of alternative techniques, such as strained materials replacing Si channel to provide higher carrier mobility [2.2], high- k dielectrics facilitating the continuously shrinking of equivalent oxide thickness (EOT) and reducing gate leakage current [2.3], new device architectures for more effectively controlling the electrostatic field in the channel [2.4], and so on. Despite lots of techniques being proposed to boost the device performance of state-of-the-art CMOSFETs, there are two basic and important features where all these techniques inevitably have to face, i.e., improved carrier transport properties relative to Si and reduced source/drain (S/D) parasitic resistance (R_{SD}) (which will be studied later in this thesis) [2.5]. Unfortunately, conventional current-voltage (I - V) modeling approaches based on drift-diffusion carrier transport in the bulk Si is inadequate to predict the electrical characteristics of short channel MOSFETs [2.6]. This is attributed to the potential quantum confinement in the vertical direction due to high impurity concentration [2.7] as well as the off-equilibrium carrier transport owing to large potential gradient along the longitudinal direction and partially quasi-ballistic transport [2.10] becoming more evident, as device dimension scales into mesoscopic regime.

Recently, Lundstrom *et al.* [2.10]–[2.14] developed a simple and analytic compact expression, based on one-flux approaches [2.15][2.16], for modeling

electrical characteristics of ultrasmall MOSFETs when channel lengths become comparable with carrier scattering mean-free-path (MFP). Fig. 2.1 shows a schematic view of channel backscattering for a MOSFET biased at high drain voltage, where the solid line represents the conduction subband energy profile. According to one-flux approaches, carrier transport from source to drain in a MOSFET can be treated as a flux with velocity (v_{inj}) injecting into a scattering matrix, where both reflection and transmission coefficients of the scattering matrix are affected by the channel potential profile [2.10]. Owing to sharp potential profile near the drain side, scattering occurred in a thickness (l_0) with an energy drop of $k_B T$ from the beginning of source-to-channel barrier primarily determines the ratio of backscattering, where part of injecting flux, r_{sat} , is scattered back to the source, and the remainder part, $1 - r_{sat}$, moves toward the drain. Once scattering occurs beyond l_0 , it is unlikely that carriers will have sufficient energy to surmount the source-to-channel barrier and return to the source [2.14]. So the total drain current is related to the amount of carriers reaching the drain. In other words, drain current is mainly controlled by two key factors in the channel backscattering theory, i.e., carrier injection velocity and channel backscattering ratio. In the following sections, we will introduce the channel backscattering theory and its current-voltage (I - V) modeling, and the methods of assessing channel backscattering ratio for comparison. Here, we will focus on a specific extraction method featuring the temperature power dependence, and deduce the related analytic expressions of calculating channel backscattering ratio under the consideration of nondegenerate and degenerate carrier statistics. Moreover, the influence of total S/D parasitic resistance on this method will also be included.

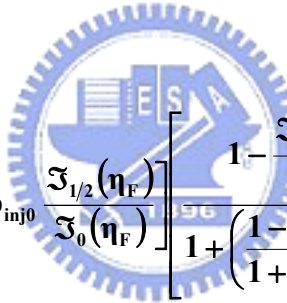
2.2 Channel Backscattering Theory and Modeling

In this section, we will introduce the full-range I - V expression with degenerate

carrier statistics, where the physical definitions of all items comprising the drain current will also be included. In addition, a compact analytic equation of saturation drain current with nondegenerate carrier statistics will be shown as well.

2.2.1 Full-Range Expression of Drain Current with Degenerate Carrier Statistics

As mentioned earlier, based on one-flux approaches introduced by Mckelvey [2.15] and Shockley *et al.* [2.16], Lundstrom *et al.* [2.10]–[2.14] developed a full-range analytic expression for modeling drain current (I_d) characteristics of a MOSFET in terms of carrier backscattering ratio (r) and injection velocity (v_{inj0}) as follows [2.11]:



$$\frac{I_d}{W} = Q_{inv}(0) \left[\frac{1-r}{1+r} \right] \left[v_{inj0} \frac{\mathfrak{F}_{1/2}(\eta_F)}{\mathfrak{F}_0(\eta_F)} \right] \left[\frac{1 - \frac{\mathfrak{F}_{1/2}(\eta_F - U_D)}{\mathfrak{F}_{1/2}(\eta_F)}}{1 + \left(\frac{1-r}{1+r} \right) \frac{\mathfrak{F}_0(\eta_F - U_D)}{\mathfrak{F}_0(\eta_F)}} \right]. \quad (2.1)$$

Eq. (2.1) is adequate for arbitrary levels of carrier degeneracy featuring the Fermi-Dirac integral $[\mathfrak{F}_n(\eta_F - U_D)]$ as a function of reduced Fermi energy (η_F) and reduced drain voltage (U_D), where η_F and U_D are defined as $\eta_F = (E_F - E_1) / k_B T$ and $U_D = qV_D / k_B T$, and E_F , E_1 , and V_D represent the Fermi level, first subband energy level and drain voltage, respectively. The I_d expression is composed of four factors, i.e., inversion charge density (Q_{inv}), ballistic efficiency (B) ($= [1 - r] / [1 + r]$, where r is the channel backscattering ratio), nondegenerate carrier injection velocity (v_{inj0}) with factor of degenerate effect $[\mathfrak{F}_{1/2}(\eta_F) / \mathfrak{F}_0(\eta_F)]$, and V_D dependence.

2.2.2 Inversion Charge Density

Here, $Q_{\text{inv}}(0)$ refers to the inversion charge density at the top of source-to-channel barrier, and can be approximately evaluated by the following expression from MOS electrostatics [2.13]

$$Q_{\text{inv}}(0) = qn_{\text{S1}}(0) \approx C_{\text{eff}}(V_{\text{G}} - V_{\text{T}}), \quad (2.1a)$$

where n_{S1} represents the carrier density in the first energy subband, and C_{eff} is the effective gate capacitance (as influenced by quantum mechanical confinement, polysilicon depletion, etc.) [2.17], and V_{G} and V_{T} are the gate and threshold voltages, respectively. In (2.1a), Lundstrom *et al.* assumed that only carriers occupying the first energy subband are included, i.e., one subband approximation. This assertion is reasonable because about 90% of the inversion carrier density and drain current arises from carriers in the first energy subband [2.13][2.18]. Moreover, it is worthy to mention that $Q_{\text{inv}}(0)$ is essentially equal to its equilibrium value in the presence or absence of channel backscattering and/or V_{D} bias, which is a key feature of self-consistent MOS electrostatics [2.14]. Based on this assumption, the device can be treated as a “well-tempered MOSFET,” which is designed to electrostatically isolate the drain from the source [2.19].

2.2.3 Channel Backscattering Ratio and Ballistic Efficiency

For nanoscale MOSFETs, it is necessary to modify the drain current equation to account for the off-equilibrium carrier transport induced by the large potential gradient across the entire channel [2.8][2.9]. On the other hand, according to the property of current continuity, the steady-state I_{d} of nanoscale MOSFETs can also be evaluated by how rapidly (e.g., v_{inj}) the carriers transport across the low-field region

near the beginning of the channel and by how many (e.g., B) carriers injecting into the channel eventually reach the drain. Here, B is to evaluate how close to the ballistic transport regime a MOSFET operates. The ideal ballistic transport means that carriers transporting from source to drain encounter no scattering events, i.e., $B=1$, however B actually ranges from zero to unity in the spirit of one-flux approaches [2.15][2.16]. The magnitude of B depends on both the scattering physics and the self-consistent potential within the channel, so B (or r) is a function of V_G and V_D [2.11]. Assuming that channel backscattering occurs in an electric-field-free semiconductor slab of length L , Lundstrom *et al.* defined r as [2.20]

$$r = \frac{1}{1 + \lambda/L}, \quad (2.1b)$$

which is further generalized to

$$r = \frac{1}{1 + \lambda/l}, \quad (2.1c)$$

where λ and l are the degenerate mean-free-path (MFP) for channel backscattering and thickness of a potential drop of $k_B T / q$ from the top of source-to-channel barrier, i.e., $k_B T$ layer thickness, with degenerate carrier statistics, respectively. Eq. (2.1b) is for a MOSFET in linear region (i.e., $V_D \ll k_B T / q$ or nearly zero electric field), while (2.1c) is for saturation region (i.e., $V_D \gg k_B T / q$) [2.21], where both λ in (2.1b) and (2.1c) are the same and defined as [2.11]

$$\lambda = \frac{2k_B T}{qv_{inj0}} \mu \frac{[\mathfrak{F}_0(\eta_F)]^2}{\mathfrak{F}_{-1}(\eta_F) \mathfrak{F}_{1/2}(\eta_F)}, \quad (2.1d)$$

where μ is the low-field carrier mobility near the source side of channel region and v_{inj0} is the nondegenerate carrier injection velocity. It is noted that even at saturation region (with high lateral electric field), λ is also affected by the low-field, quasi-equilibrium μ in the source, owing to the property of current continuity, as stated above [2.14]. Here, carriers in the source-side is under quasi-equilibrium since the energy gain experienced by carriers is no more than about $k_B T / q$ as channel backscattering occurs [2.10], which is also verified by Monte Carlo simulation [2.22]. Furthermore, Lundstrom *et al.* also refers to λ as the MFP for channel backscattering rather than MFP itself, where more details can be found in [2.14].

In the channel backscattering model, the steady-state I_d is limited only by channel backscattering that occurs within a critical length l , where the potential drop from the peak of source-to-channel barrier is $k_B T / q$ and was first noted by Price [2.23]. Performing Monte Carlo simulations of carrier transport down a potential barrier, Price observed that once carriers penetrated even only a very short distance into the potential drop, carriers were unlikely to return to the original injection point even if they did scatter. Similarly, for a metal-semiconductor junction, Bethe [2.24] showed that thermionic-limited current occurs, when the potential drop of first $k_B T / q$ at the junction occurs over a distance much less than the carrier MFP. Here, the degenerate l is defined as [2.11]

$$l = \beta \frac{k_B T}{q \varepsilon(0)}, \quad (2.1e)$$

where $\varepsilon(0)$ is the electric field at the top of source-to-channel barrier, and β is a numerical factor ($\beta \cong 1$ for nondegenerate carrier statistics, and is slightly larger than

unity for the degenerate case).

2.2.4 Carrier Injection Velocity

Except the ballistic efficiency (or channel backscattering ratio), carrier injection velocity is a critical parameter in determining the drain current. The degenerate v_{inj} is defined as follows

$$v_{inj} = v_{inj0} \frac{\mathfrak{F}_{1/2}(\eta_F)}{\mathfrak{F}_0(\eta_F)} = \sqrt{\frac{2k_B T}{\pi m^*}} \frac{\mathfrak{F}_{1/2}(\eta_F)}{\mathfrak{F}_0(\eta_F)}, \quad (2.1f)$$

where v_{inj0} is for nondegenerate carrier statistics, and m^* is the carrier effective mass. So the carrier injection velocity is almost constant and approximately equals to the carrier thermal velocity ($\approx 1.2 \times 10^7$ cm/s) at low carrier density, but significantly increases with the V_G once carriers become degenerate (or $V_G > V_T$) [2.14].

2.2.5 Compact Analytic Model of Saturation Drain Current

Removing the factors of degenerate carrier statistics from (2.1), we can deduce a full-range nondegenerate analytic model as follows

$$\frac{I_d}{W} = Q_{inv}(0) \frac{1-r_0}{1+r_0} v_{inj0} \left[\frac{1-e^{-U_D}}{1+\left(\frac{1-r_0}{1+r_0}\right)e^{-U_D}} \right], \quad (2.2)$$

where r_0 represents the nondegenerate channel backscattering ratio. Furthermore, when the MOSFET is operating under saturation region, the V_D -dependent factor in

the bracket of (2.2) is close to unity, and then (2.2) can be reduce as follows:

$$\frac{I_{\text{dsat}}}{W} = Q_{\text{inv}}(0) \frac{1 - r_{\text{sat0}}}{1 + r_{\text{sat0}}} v_{\text{inj0}} = Q_{\text{inv}}(0) v_{\text{inj0}} B_{\text{sat0}}, \quad (2.3)$$

where I_{dsat} is the saturation drain current, and r_{sat0} and B_{sat0} are the nondegenerate channel backscattering ratio and ballistic efficiency at saturation region. Eq. (2.3) is the compact expression of (2.1). So at a given Q_{inv} , both ballistic efficiency and carrier injection velocity are critical parameters in determining the saturation drain current.

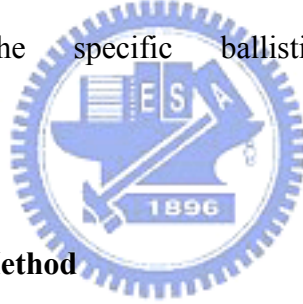
2.3 Extraction of Channel Backscattering Ratio

The channel backscattering ratio (or ballistic efficiency) is used to evaluate how close to the ballistic transport limit the MOSFET operates by modifying fabrication processes and/or device architectures. There are some techniques, such as fitting ballistic model to measured I - V characteristics [2.21][2.25][2.26], transconductance method [2.8][2.9], drain current method [2.27], and temperature-dependent analytic method [2.26][2.28], for assessing the channel backscattering ratio. In this section, we will briefly introduce the first three techniques and compare with each other, whereas the last one, adopted in this work, will be discussed in detail in Section 2.4.

2.3.1 Fitting Ballistic Model to Measured Current–Voltage Characteristics

This extraction method is to reproduce experimental measured I - V characteristics by simulated ballistic current. First, by inputting some process parameters, such as physical oxide thickness (t_{OX}), bulk doping concentration (N_{B}), and poly-Si gate doping concentration (N_{Poly}), into a self-consistent

Schrödinger-Poisson simulator, the Q_{inv} and v_{inj} can be calculated [2.21][2.25][2.26]. Then, the drain current at ballistic transport limit can also be obtained from (2.3) with the input of B_{sat} being equal to unity. Here, fitting the experimental measured $I-V$ characteristics by simulated ballistic current with an iteratively modulated B_{sat} , we can find the r_{sat} (or B_{sat}) of the characterized MOSFET until the simulated $I-V$ exactly reproduces the measured one. Since this technique evaluates the r_{sat} (or B_{sat}) directly from simulations, it is free from the extraction complexities probably experienced by pure experimental extraction methodology (as introduced later). In addition, by virtue of simulation the effect of degenerate carrier statistics involving complicated numerical calculations can be also included for r_{sat} evaluation. However, the $I-V$ equation of each ballistic model is not entirely the same, which results in the r_{sat} value being dependent on the specific ballistic $I-V$ model employed [2.7][2.11][2.18][2.29][2.30].



2.3.2 Transconductance Method

This technique first evaluates the v_{inj0} according to the following equations [2.8][2.9]

$$v_{inj0} = \frac{G_{mi}}{WC_{eff}}, \quad (2.4)$$

where G_{mi} is the intrinsic peak transconductance of the MOSFET, and can be obtained from the measured maximum transconductance (G_m) with $G_{mi} = G_m / (1 - 0.5R_{SD}G_m - R_{SD}G_D)$ [2.8], where G_D and R_{SD} are the output conductance and total source/drain (S/D) parasitic resistance, respectively. As the MOSFET reaches the ballistic transport limit, carrier injection velocity is assumed to be equal to the thermal velocity (v_{th} ,

$1.2 - 2 \times 10^7$ cm/s) from the source accumulation layer into the channel [2.20][2.21], and then B_{sat0} can be treated as a gap of extracted v_{inj} to v_{th} as the following expression [2.18]

$$B_{\text{sat0}} = \frac{v_{\text{inj0}}}{v_{\text{th}}}, \quad (2.5)$$

where v_{th} is the thermal velocity as mentioned above.

2.3.3 Drain Current Method

Similar to the transconductance method, drain current method estimates the B_{sat0} by (2.5), whereas the v_{inj0} is extracted by the following expression [2.27]



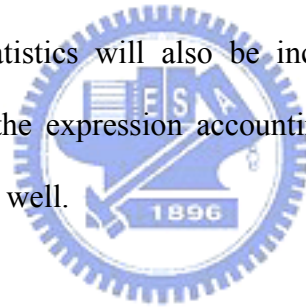
$$v_{\text{inj0}} = \frac{I_{\text{dsat}}}{W \int C_{\text{eff}} dV_G}, \quad (2.6)$$

where the integral in the denominator represents the Q_{inv} at saturation region. Here, based on the above statement, both transconductance and drain current methods can be employed to find r_{sat0} by (2.4)–(2.6) easily, but there are still some issues for estimating r_{sat0} . Firstly, once the extracted v_{inj0} exceeds the thermal velocity, the magnitude of B_{sat0} from (2.5) will be larger than unity, which violates the key assumption of one-flux approaches, i.e., $0 \leq B_{\text{sat0}} \leq 1$, and is unreasonable in physics. Secondly, both extraction techniques generally overestimate B_{sat0} (or underestimate r_{sat0}) because the extracted v_{inj0} is more close to the average carrier velocity in the channel rather than the carrier velocity at the peak of source-to-channel barrier [2.7][2.31]. The higher carrier velocity in the channel is ascribed to the fact that

carriers already start to be accelerated by the potential profile. That is, larger extraction error will be induced as long as the position of source-to-channel barrier peak is shifted toward the drain more, which is confirmed by energy balance simulations [2.31].

2.4 Temperature-Dependent Analytic Model for Extracting Channel Backscattering Ratio

In this section, we introduce an extraction technique of evaluating the channel backscattering ratio by a temperature-dependent analytic expression based on scattering theory [2.10]–[2.14]. Firstly, an analytic expression with nondegenerate carrier statistics will be deduced step by step. Secondly, the expression with degenerate-limited carrier statistics will also be included and compared with the nondegenerate one. Finally, the expression accounting for the influence of R_{SD} on drain current will be shown as well.



2.4.1 Nondegenerate Carrier Statistics

In references [2.26] and [2.28], it was demonstrated that by measuring saturation drain current against a range of temperature, the channel backscattering ratio (or ballistic efficiency) as a function of the ratio of carrier MFP for channel backscattering (λ_0) to $k_B T$ layer thickness (l_0), as shown in (2.1c), at a specific temperature (T) can be simply extracted. Here, we employ the full-range nondegenerate I – V expression [2.11], as shown in (2.2), and differentiate the drain current expression with respect to T as follows

$$\begin{aligned}
\frac{\partial I_d}{\partial T} &= \frac{\partial}{\partial T} \left[WC_{\text{eff}} v_{\text{inj}0} \frac{1-r_0}{1+r_0} (V_G - V_T) \frac{1-e^{-U_D}}{1+\left(\frac{1-r_0}{1+r_0}\right)e^{-U_D}} \right] \\
&= I_d \left[\frac{1}{v_{\text{inj}0}} \frac{\partial v_{\text{inj}0}}{\partial T} + \frac{1+r_0}{1-r_0} \frac{\partial}{\partial T} \left(\frac{1-r_0}{1+r_0} \right) + \frac{1}{V_G - V_T} \frac{\partial (V_G - V_T)}{\partial T} - \frac{U_D e^{-U_D}}{1-e^{-U_D}} \frac{1}{T} \right] \\
&\quad - I_d \left[\frac{e^{-U_D}}{1+\left(\frac{1-r_0}{1+r_0}\right)e^{-U_D}} \left(\frac{1-r_0}{1+r_0} \right) \left(\frac{U_D}{T} - \left(\frac{1}{1+r_0} + \frac{1}{1-r_0} \right) \frac{\partial r_0}{\partial T} \right) \right] \\
&= \alpha I_d, \tag{2.7}
\end{aligned}$$

where U_D is the reduced drain voltage and defined as $U_D = qV_D / k_B T$. In this work, we only consider the situation where the MOSFET is biased at saturation region, i.e., $V_D \gg k_B T / q$ [2.11]. Then, (2.7) can be further reduced as follows

$$\begin{aligned}
\frac{\partial I_{\text{dsat}}}{\partial T} &= I_{\text{dsat}} \left[\frac{1}{v_{\text{inj}0}} \frac{\partial v_{\text{inj}0}}{\partial T} + \frac{1+r_{\text{sat}0}}{1-r_{\text{sat}0}} \frac{\partial}{\partial T} \left(\frac{1-r_{\text{sat}0}}{1+r_{\text{sat}0}} \right) + \frac{1}{V_G - V_{T,\text{sat}}} \frac{\partial (V_G - V_{T,\text{sat}})}{\partial T} \right] \\
&= \alpha I_{\text{dsat}}, \tag{2.8}
\end{aligned}$$

where the exponent of order $-U_D$ approaches zero and is removed in (2.8). Then, according to [2.20], the items comprising the I_{dsat} have the following power dependence of temperature: the carrier injection velocity $v_{\text{inj}0} \propto T^{-1/2}$; the carrier MPF for channel backscattering $\lambda_0 \propto T^{-1}$; $k_B T$ layer thickness $l_0 \propto T$; and the low-field carrier mobility $\mu_0 \propto T^{-3/2}$. Based on these temperature dependences, the derivatives of $v_{\text{inj}0}$ and $r_{\text{sat}0}$ are deduced as follows: $\partial v_{\text{inj}0} / \partial T = v_{\text{inj}0} / 2T$ and $\partial r_{\text{sat}0} / \partial T = 2r_{\text{sat}0}(1 - r_{\text{sat}0}) / T$. Substituting these two derivatives into (2.8), we obtain the following results [2.32]

$$\begin{aligned}
\frac{\partial I_{\text{dsat}}}{\partial T} &= I_{\text{dsat}} \left[\frac{1}{2T} - \left(\frac{1}{1+r_{\text{sat0}}} + \frac{1}{1-r_{\text{sat0}}} \right) \frac{\partial r_{\text{sat0}}}{\partial T} - \frac{\eta}{V_G - V_{T,\text{sat}}} \right] \\
&= I_{\text{dsat}} \left[\frac{1}{2T} - \frac{4r_{\text{sat0}}}{(1+r_{\text{sat0}})T} - \frac{\eta}{V_G - V_{T,\text{sat}}} \right] \\
&= I_{\text{dsat}} \left[\frac{1}{T} \left(\frac{1}{2} - \frac{4}{2+\lambda_0/l_0} \right) - \frac{\eta}{V_G - V_{T,\text{sat}}} \right] \\
&= \alpha I_{\text{dsat}}, \tag{2.9}
\end{aligned}$$

where α and η represent the temperature coefficients of I_{dsat} and $V_{T,\text{sat}}$, respectively, i.e., $\alpha = \partial I_{\text{dsat}} / (I_{\text{dsat}} \partial T)$ and $\eta = \partial V_{T,\text{sat}} / \partial T$. Rearranging (2.9), we obtain an analytic expression of λ_0 / l_0 in terms of α , η , V_G , and $V_{T,\text{sat}}$ at a specific temperature T as follows

$$\lambda_0 / l_0 = \frac{4}{0.5 - \left(\frac{\eta}{V_G - V_{T,\text{sat}}} + \alpha \right) T} - 2. \tag{2.10}$$

Fig. 2.2 shows the flow chart of temperature-dependent extraction technique for estimating the r_{sat0} (or B_{sat0}). This technique utilizes the temperature-dependent property to deduce a simple and analytic expression for evaluating the r_{sat0} directly from experimental I - V characteristics without involving the complication issues, as discussed in Section 2.3.

2.4.2 Degenerate-Limited Carrier Statistics

Eq. (2.10) is adequate only for a MOSFET operating at low inversion carrier densities ($n_s < 10^{12} \text{ cm}^{-2}$) or at low V_G ($V_G < V_T$). When n_s becomes comparable to 10^{13} cm^{-2} (or the MOSFET is biased at high V_G , i.e., $V_G > V_T$), the effect of carrier degeneracy causes the channel backscattering factors to be significantly affected not

only by T but also V_G [2.12]. The extraction expression for I_{dsat} with degenerate carrier statistics can be deduced similarly, albeit more complicated mathematics will be involved in the deduction. Therefore, the limit of carrier degeneracy, i.e., $\eta_F \rightarrow \infty$, is assumed here for simplicity [2.13]. Then, the limit of degenerate carrier injection velocity (v_{inj}), degenerate carrier MFP for channel backscattering (λ), and degenerate channel backscattering ratio (r_{sat}) can be reduced as follows:

$$\begin{aligned}
\lim_{\eta_F \rightarrow \infty} v_{\text{inj}} &= \lim_{\eta_F \rightarrow \infty} \sqrt{\frac{2k_B T}{\pi m^*} \frac{\mathfrak{S}_{1/2}(\eta_F)}{\mathfrak{S}_0(\eta_F)}} = \lim_{\eta_F \rightarrow \infty} \sqrt{\frac{2k_B T}{\pi m^*} \frac{\mathfrak{S}_{1/2}(\eta_F)}{\ln(1 + e^{\eta_F})}} \\
&= \frac{4}{3} \sqrt{\frac{2k_B T \eta_F}{\pi^2 m^*}} = \frac{4\hbar}{3m^*} \sqrt{\frac{2C_{\text{eff}}(V_G - V_T)}{\pi q}} \\
&= A' \sqrt{V_G - V_T}, \tag{2.11a}
\end{aligned}$$

$$\begin{aligned}
\lim_{\eta_F \rightarrow \infty} \lambda &= \lim_{\eta_F \rightarrow \infty} \frac{\sqrt{2\pi m^* k_B T} \mu_0 [\mathfrak{S}_0(\eta_F)]^2}{q \mathfrak{S}_{-1}(\eta_F) \mathfrak{S}_{1/2}(\eta_F)} \\
&= \lim_{\eta_F \rightarrow \infty} \frac{\sqrt{2\pi m^* k_B T} \mu_0 [\ln(1 + e^{\eta_F})]^2}{q e^{\eta_F} (1 + e^{\eta_F})^{-1} \mathfrak{S}_{1/2}(\eta_F)} \\
&= \frac{\sqrt{2\pi m^* k_B T}}{q} \mu_0 \frac{3\sqrt{\pi \eta_F}}{4} = \frac{3\sqrt{2\pi^2 m^* k_B T \eta_F}}{4q} \mu_0 \\
&= B' T^{-1.5} \sqrt{V_G - V_T}, \tag{2.11b}
\end{aligned}$$

and

$$\begin{aligned}
\lim_{\eta_F \rightarrow \infty} r &= \lim_{\eta_F \rightarrow \infty} (1 + \lambda/l)^{-1} = \lim_{\eta_F \rightarrow \infty} \left(1 + \frac{\varepsilon(0)\mu_0}{\beta} \sqrt{\frac{2\pi m^*}{k_B T}} \frac{[\mathfrak{F}_0(\eta_F)]^2}{\mathfrak{F}_{-1}(\eta_F)\mathfrak{F}_{1/2}(\eta_F)} \right)^{-1} \\
&= \lim_{\eta_F \rightarrow \infty} \left(1 + \frac{\varepsilon(0)\mu_0}{\beta} \sqrt{\frac{2\pi m^*}{k_B T}} \frac{[\ln(1 + e^{\eta_F})]^2}{e^{\eta_F}(1 + e^{\eta_F})^{-1}\mathfrak{F}_{1/2}(\eta_F)} \right)^{-1} \\
&= \left(1 + \frac{3\varepsilon(0)\mu_0}{4\beta} \sqrt{\frac{2\pi^2 m^* \eta_F}{k_B T}} \right)^{-1} \\
&= \left(1 + C'T^{-2.5} \sqrt{V_G - V_T} \right)^{-1}. \tag{2.11c}
\end{aligned}$$

where $\mathfrak{F}_n(\eta_F)$ is the Fermi-Dirac integral with order n , as stated earlier, and η_F is the reduced Fermi energy and defined as $\eta_F = (E_F - E_1) / k_B T$. At the limit of carrier degeneracy, i.e., $E_F \gg E_1$ (or at large V_G), $\mathfrak{F}_n(\eta_F)$ can be simplified and expressed in terms of $(V_G - V_T)$ [2.33], where the channel backscattering model assumes that carriers only occupy the first energy subband, and then total inversion charge density can be expressed as $Q_{\text{inv}} = qn_s = C_{\text{eff}}(V_G - V_T) = qm^*(E_F - E_1) / \pi \hbar^2$ (\hbar is the reduced Planck constant) [2.13]. Based on this assumption, (2.11a)–(2.11c) can be reduced as a function of $(V_G - V_T)$ and T , where A' , B' , and C' are constants. In (2.11c), the degenerate $k_B T$ layer thickness (l) is defined as $l = \beta(k_B T / q)$, where β is a constant and slightly larger than unity [2.11]. Differentiating (2.11a)–(2.11c) with respect to T , we can modify (2.8) as follows

$$\begin{aligned}
\frac{\partial I_{\text{dsat}}}{\partial T} &= I_{\text{dsat}} \left[\frac{1}{v_{\text{inj}}} \frac{\partial v_{\text{inj}}}{\partial T} \Big|_{\eta_F \rightarrow \infty} + \frac{1+r_{\text{sat}}}{1-r_{\text{sat}}} \frac{\partial}{\partial T} \left(\frac{1-r_{\text{sat}}}{1+r_{\text{sat}}} \right) \Big|_{\eta_F \rightarrow \infty} + \frac{1}{V_G - V_{T,\text{sat}}} \frac{\partial (V_G - V_{T,\text{sat}})}{\partial T} \right] \\
&= I_{\text{dsat}} \left[-\frac{0.5\eta}{V_G - V_{T,\text{sat}}} - r_{\text{sat}} \left(1 + \frac{1-r_{\text{sat}}}{1+r_{\text{sat}}} \right) \left(\frac{2.5}{T} + \frac{0.5\eta}{V_G - V_{T,\text{sat}}} \right) - \frac{\eta}{V_G - V_{T,\text{sat}}} \right] \\
&= \alpha I_{\text{dsat}}, \tag{2.12}
\end{aligned}$$

where $\frac{\partial r_{\text{sat}}}{\partial T} \Big|_{\eta_F \rightarrow \infty} = r_{\text{sat}}(1-r_{\text{sat}}) \left(\frac{2.5}{T} + \frac{0.5\eta}{V_G - V_{T,\text{sat}}} \right)$, and the definitions of α and η are

the same as those of (2.9). After rearrangements, the analytic expression with degenerate-limited carrier statistics is given as follows

$$\lambda/l = - \left[\left(\frac{5}{T} + \frac{\eta}{V_G - V_{T,\text{sat}}} \right) / \left(\alpha + \frac{1.5\eta}{V_G - V_{T,\text{sat}}} \right) + 2 \right]. \quad (2.13)$$

2.4.3 Consideration of Source/Drain Parasitic Resistance

The I - V equation, as shown in (2.3), neglects the influence of total source/drain (S/D) parasitic resistance (R_{SD}) on current performance. In reality, significant degradation of drain current, e.g., 30% decrease of I_{dsat} [2.21], is observed when R_{SD} is taken into consideration. Therefore, we modify (2.3) with the effect of R_{SD} as follows

$$I_{\text{dsat}} = WC_{\text{eff}} v_{\text{inj}0} \frac{1 - r_{\text{sat}0}}{1 + r_{\text{sat}0}} \left[(V_G - 0.5I_{\text{dsat}}R_{SD}) - (V_{T,\text{lin}} - \Delta V_{\text{DIBL}}(V_D - I_{\text{dsat}}R_{SD})) \right], \quad (2.14)$$

where the terms $(V_G - 0.5I_{\text{dsat}}R_{SD})$ and $(V_D - I_{\text{dsat}}R_{SD})$ are the intrinsic V_G and intrinsic V_D , respectively, and the term $(V_{T,\text{lin}} - \Delta V_{\text{DIBL}}(V_D - I_{\text{dsat}}R_{SD}))$ represents the saturation threshold voltage later designated as $V_{T,\text{sat}}$ [2.26]. In addition, $V_{T,\text{lin}}$ is the linear threshold voltage and is determined by maximum transconductance method, and ΔV_{DIBL} is the V_G difference between linear and saturation region by constant current method. Then, differentiating (2.14) with respect to T , we obtain the following expression

$$\frac{\partial I_{\text{dsat}}}{\partial T} = I_{\text{dsat}} \left[\frac{1}{v_{\text{inj0}}} \frac{\partial v_{\text{inj0}}}{\partial T} + \frac{1+r_{\text{sat0}}}{1-r_{\text{sat0}}} \frac{\partial}{\partial T} \left(\frac{1-r_{\text{sat0}}}{1+r_{\text{sat0}}} \right) \right] + \frac{I_{\text{dsat}}}{P} \left[-0.5R_{\text{SD}} \frac{\partial I_{\text{dsat}}}{\partial T} - \frac{\partial V_{\text{T,lin}}}{\partial T} + (V_{\text{D}} - I_{\text{dsat}}R_{\text{SD}}) \frac{\partial \Delta V_{\text{DIBL}}}{\partial T} - R_{\text{SD}} \Delta V_{\text{DIBL}} \frac{\partial I_{\text{dsat}}}{\partial T} \right]. \quad (2.15)$$

In (2.15), we temporarily assign “ P ” to represent the expression in the bracket of (2.14), i.e., $[(V_{\text{G}} - 0.5I_{\text{dsat}}R_{\text{SD}}) - (V_{\text{T,lin}} - \Delta V_{\text{DIBL}} (V_{\text{D}} - I_{\text{dsat}}R_{\text{SD}}))]$, for simplifying the expression. By further rearranging (2.15), we can obtain the following result

$$\frac{\partial I_{\text{dsat}}}{\partial T} = \frac{\frac{I_{\text{dsat}}}{T} \left(0.5 - \frac{4}{2 + \lambda_0/l_0} \right) + \frac{I_{\text{dsat}}}{P} \left((V_{\text{D}} - I_{\text{dsat}}R_{\text{SD}}) \frac{\partial \Delta V_{\text{DIBL}}}{\partial T} - \frac{\partial V_{\text{T,lin}}}{\partial T} \right)}{1 + \frac{0.5I_{\text{dsat}}R_{\text{SD}} + I_{\text{dsat}}R_{\text{SD}}\Delta V_{\text{DIBL}}}{P}} = I_{\text{dsat}} \alpha, \quad (2.16)$$

where α is shown as follows

$$\alpha = \frac{\frac{1}{T} \left(0.5 - \frac{4}{2 + \lambda_0/l_0} \right) P + (V_{\text{D}} - I_{\text{dsat}}R_{\text{SD}}) \frac{\partial \Delta V_{\text{DIBL}}}{\partial T} - \frac{\partial V_{\text{T,lin}}}{\partial T}}{V_{\text{G}} - V_{\text{T,lin}} + \Delta V_{\text{DIBL}} V_{\text{D}}}. \quad (2.16')$$

From (2.16') the analytic expression of λ_0 / l_0 with R_{SD} effect for evaluating the r_{sat0} (or B_{sat0}) has the following expression

$$\frac{4}{2 + \lambda_0/l_0} = 0.5 - T \frac{\alpha (V_{\text{G}} - V_{\text{T,lin}} + V_{\text{D}} \Delta V_{\text{DIBL}}) - (V_{\text{D}} - I_{\text{dsat}}R_{\text{SD}}) \frac{\partial \Delta V_{\text{DIBL}}}{\partial T} + \frac{\partial V_{\text{T,lin}}}{\partial T}}{(V_{\text{G}} - 0.5I_{\text{dsat}}R_{\text{SD}}) - (V_{\text{T,lin}} - \Delta V_{\text{DIBL}} (V_{\text{D}} - I_{\text{dsat}}R_{\text{SD}}))}. \quad (2.17)$$

2.5 Conclusions

In this chapter, we introduce the theory and current-voltage modeling of channel backscattering. Firstly, a full-range drain current expression with degenerate carrier statistics is shown. The meaning of the related items constituting the current expression, i.e., inversion charge density, channel backscattering ratio, ballistic efficiency, carrier mean-free-path for channel backscattering, $k_B T$ layer thickness and carrier injection velocity, are physically defined. Secondly, for a MOSFET being biased at saturation region with the assumption of nondegenerate carrier statistics, we can reduce the full-range degenerate current expression to a compact one. From the compact analytic expression, it is noted that for a given inversion charge density both ballistic efficiency and carrier injection velocity are critical parameters in determining the drain current, where the ballistic efficiency is also employed to evaluate how close to ballistic transport limit a MOSFET operates. Thirdly, we show some techniques of assessing the ballistic efficiency and make comparisons with each other. Among these extraction techniques, we adopt the technique of utilizing the power dependence of temperature and deduce an analytic expression for evaluating the nondegenerate channel backscattering ratio and/or ballistic efficiency. Similarly, the expression with degenerate-limited carrier statistics is also deduced for comparison. Finally, the influence of total source/drain parasitic resistance on drain current is taken into consideration in the analytic expression as well.

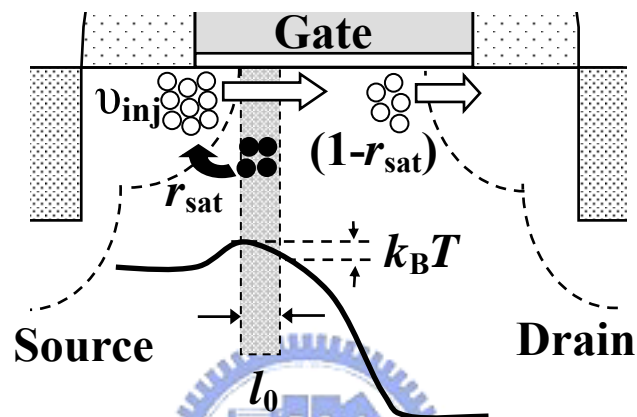


Fig. 2.1. Schematic diagram of channel backscattering phenomenon in a MOSFET. When carriers are injected from source into channel, they may encounter scattering within a short distance l_0 with a potential drop of $k_B T / q$ beginning from the top of source-to-channel barrier. Some carriers (r_{sat}) may be scattered back to the source, and the remaining carriers $(1 - r_{sat})$ reach the drain.

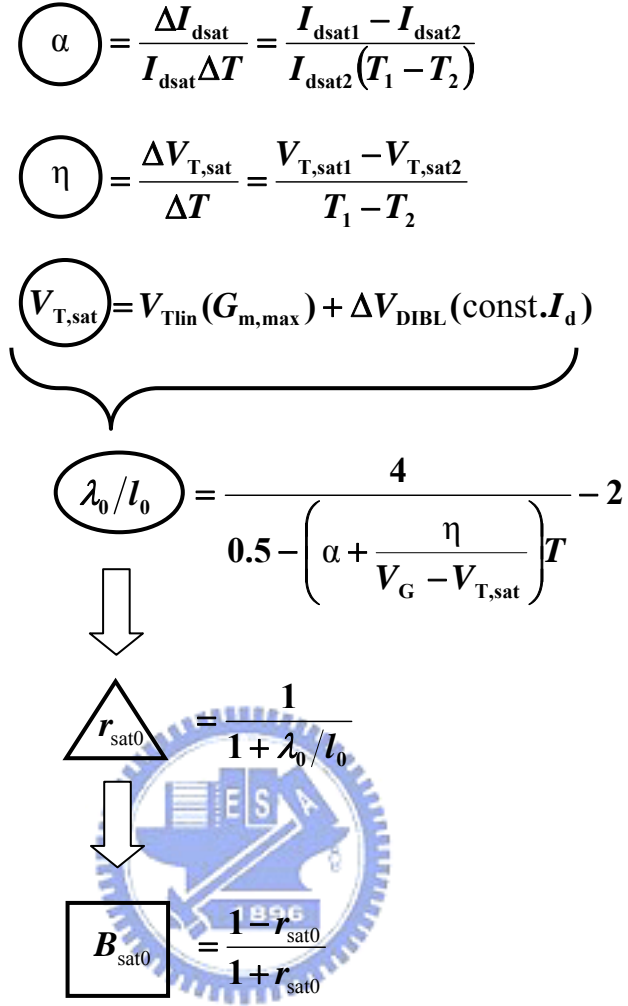


Fig. 2.2. Flow chart of temperature-dependent extraction technique for evaluating channel backscattering ratio (r_{sat0}) and ballistic efficiency (B_{sat0}). The α and η represent the temperature coefficients of saturation drain current (I_{dsat}) and threshold voltage ($V_{\text{T,sat}}$), respectively, where $V_{\text{T,sat}}$ is determined by maximum transconductance ($G_{\text{m,max}}$) method with drain-induced barrier lowering (DIBL, ΔV_{DIBL}) consideration. By extracting α , η and $V_{\text{T,sat}}$, we can calculate the ratio of channel backscattering mean-free-path (MFP, λ_0) to $k_{\text{B}}T$ layer thickness (l_0), so r_{sat0} and B_{sat0} can be calculated.